Article

Current Biology

Whi3 mnemon association with endoplasmic reticulum membranes confines the memory of deceptive courtship to the yeast mother cell

Highlights

- Whi3 mnemon associates with endoplasmic reticulum membranes
- Diffusion barriers restricts Whi3 mnemon inheritance to the mother cell
- Whi3 prion-like domain can assemble in self-templating fibrils *in vitro*
- Whi3 can adopt a prion-like behavior in diffusion barrier-defective cells

Authors

Yasmin Lau, Henry Patrick Oamen, Marcel Grogg, ..., Donald Hilvert, Yves Barral, Fabrice Caudron

Correspondence

fabrice.caudron@igmm.cnrs.fr

In brief

Lau et al. identify that the self-templating yeast mnemon Whi3 is retained in the mother cell during cell division after the memorization of a deceptive mating attempt through an association with compartmentalized endoplasmic reticulum membranes. This confinement is required to prevent the appearance of a mitotically stable prion-like behavior of Whi3.

Lau et al., 2022, Current Biology *32*, 963–974
March 14, 2022
https://doi.org/10.1016/j.cub.2022.01.002

CellPress

Current Biology

CellPress
OPEN ACCESS

Article

Whi3 mnemon association with endoplasmic reticulum membranes confines the memory of deceptive courtship to the yeast mother cell

Yasmin Lau,[1,8] Henry Patrick Oamen,[1,8] Marcel Grogg,[2] Iuliia Parfenova,[3] Juha Saarikangas,[4,5,6] Robin Hannay,[1] Richard Alan Nichols,[1] Donald Hilvert,[2] Yves Barral,[3] and Fabrice Caudron[1,7,9,10,*]

[1]School of Biological and Behavioural Sciences, Queen Mary University of London, Mile End Road, London E1 4NS, UK
[2]Laboratory of Organic Chemistry, ETH Zürich, Vladimir-Prelog-Weg, 8093 Zürich, Switzerland
[3]Institute of Biochemistry, ETH Zürich, Otto-Stern-Weg, 8093 Zürich, Switzerland
[4]Helsinki Institute of Life Science HiLIFE, Viikinkaari 5, 00790 Helsinki, Finland
[5]Faculty of Biological and Environmental Sciences, Viikinkaari 5, 00790 Helsinki, Finland
[6]Neuroscience Center, University of Helsinki, Viikinkaari 5, 00790 Helsinki, Finland
[7]IGMM, Univ Montpellier, CNRS, Route de Mende, 34293 Montpellier, France
[8]These authors contributed equally
[9]Twitter: @Caudronfabrice1
[10]Lead contact
*Correspondence: fabrice.caudron@igmm.cnrs.fr
https://doi.org/10.1016/j.cub.2022.01.002

SUMMARY

Prion-like proteins are involved in many aspects of cellular physiology, including cellular memory. In response to deceptive courtship, budding yeast escapes pheromone-induced cell-cycle arrest through the coalescence of the G1/S inhibitor Whi3 into a dominant, inactive super-assembly. Whi3 is a mnemon (Whi3^{mnem}), a protein that conformational change maintains as a trait in the mother cell but is not inherited by the daughter cells. How the maintenance and asymmetric inheritance of Whi3^{mnem} are achieved is unknown. Here, we report that Whi3^{mnem} is closely associated with endoplasmic reticulum (ER) membranes and is retained in the mother cell by the lateral diffusion barriers present at the bud neck. Strikingly, barrier defects made Whi3^{mnem} propagate in a mitotically stable, prion-like manner. The amyloid-forming glutamine-rich domain of Whi3 was required for both mnemon and prion-like behaviors. Thus, we propose that Whi3^{mnem} is in a self-templating state, lending temporal maintenance of memory, whereas its association with the compartmentalized membranes of the ER prevents infectious propagation to the daughter cells. These results suggest that confined self-templating super-assembly is a powerful mechanism for the long-term encoding of information in a spatially defined manner. Yeast courtship may provide insights on how individual synapses become potentiated in neuronal memory.

INTRODUCTION

Prions are proteins that can adopt several conformations, at least one of which is self-templating, lending it a self-perpetuating character and supporting its propagation in the cell population, or even across individuals, in an infectious-like manner. Therefore, although prion conversion is essential for physiological processes including innate immunity[1] and the generation of the phenotypic diversity of single-celled organisms,[2–4] prion propagation may also lead to disease states. Accordingly, prions were initially discovered as the agents of human (Kuru, Creutzfeldt-Jakob's disease) and animal diseases (Scrapie and Bovine spongiform encephalopathy).[5] Moreover, prion-like behavior may be linked to degenerative conditions[6] and contribute to the resistance of pathogenic yeasts to antifungal drugs.[7] The mechanisms controlling prions and particularly their self-templating activity are still open questions.

Interestingly, recent studies reveal the role of prion-like proteins in spatially defined processes, i.e., where conversion is not associated with an infectious-like propagation of the protein. Such an instance occurs during the response of yeast cells to pheromone: upon the detection of the pheromone produced by the cells of the opposite mating type, haploid yeast cells arrest in the G1 phase of the cell cycle and grow toward the source of this signal. If no partner is reached within a reasonable time, i.e., in deceptive courtship, yeast cells become refractory to the pheromone signal and resume vegetative proliferation.[8,9] Remarkably, once established, this pheromone refractory state is stable, lending memory to the cell that there is no partner available for the remainder of their lifespan. Strikingly, daughter cells do not inherit this refractory state, restoring their ability to respond to pheromone upon separation from the mother cell.[8] Thus, yeast courtship provides a simple model for studying how single cells keep memory of past events and use this information to individually adapt their behavior to their environment.

Remarkably, the condensation of the Whi3 protein into a super-assembly state drives the escape from pheromone arrest

and the establishment of the refractory state upon deceptive courtship.[8] This behavior relies on prion-like domains in the Whi3 protein, which is composed of polyQ- and polyN-rich stretches.[8,10] In its soluble state, Whi3 regulates the G1/S transition of the cell cycle through binding and inhibiting the translation of the G1 cyclin *CLN3* mRNA.[11] This inhibition ensures that the entry into S phase is delayed until cells reach a critical size and contributes to cell-cycle arrest in response to pheromone. Upon deceptive courtship, Whi3 condensation releases the *CLN3* mRNA from inhibition and triggers the return of the cell to the proliferation cycle. However, how the refractory state is subsequently maintained over time by individual cells is unknown.

Whi3's domain organization and ability to switch to a condensed phase are features that it shares with prions. This suggests that the condensed state of Whi3 might be self-templating, lending an attractive model for how the dominant effect of Whi3^{mnem} might be maintained. However, whether the condensed state of Whi3 indeed shows self-templating properties is unknown. Furthermore, this possibility would raise the question of why this state does not propagate mitotically to the daughter cells as prions, including the eRF3 translation terminator Sup35 protein in its prion form [*PSI*$^{+}$], do.[8,12] Thus, the behavior of the Whi3 protein during memory maintenance raises the question of how cells stabilize memory in the long term and spatially restrict it to individual cells or subcellular locations.

To address this question, here, we investigated what distinguishes the Whi3 mnemon from yeast prions such as Sup35.

RESULTS

Whi3 super-assemblies and Sup35 foci differ in their association with ER membranes

To understand what distinguishes mnemons from prions, we compared the subcellular localization of Whi3 and Sup35. During cell division, Whi3 granules associate with endoplasmic reticulum (ER) membranes.[13] To test whether Sup35 and Whi3 differ in their association with cellular membranes, we analyzed the localization of Sup35, in its [*PSI*$^{+}$] prion form, and the Whi3^{mnem} super-assemblies relative to the ER. ER membranes were visualized using the translocon subunit Sec61 tagged with mCherry. In [*PSI*$^{+}$] cells, a fraction of the foci formed by the Sup35 fused to a GFP was associated with ER membranes as reported,[14] but the majority of those were spatially separated from the Sec61 signal (Figures 1A and 1B, 53.1% ±10.7% of Sup35-GFP foci were away from the Sec61-mCherry signal). Indeed, 100% of [*PSI*$^{+}$] cells contained at least one Sup35-GFP focus away from ER membranes.

In contrast to Sup35-GFP, the cells expressing Whi3 fused to mNeonGreen (Whi3-mNG) and exposed to pheromone for 3 h formed super-assemblies mainly in contact with ER membranes (72.5% ± 4.1% of super-assemblies, Figures 1D and 1H). Accordingly, Whi3 partly cofractionated with the microsomes in the lysates of cells before and after pheromone treatment (Figure 1C). The fraction of Whi3 super-assemblies associated with the ER increased upon longer pheromone exposure (82.7% ± 2.1% after 4 h, 90.0% ± 3.5% after 6 h, and 92.1% ± 3.2% after 10.5 h; Figures 1E–1H). Remarkably, while 41.2% ± 9.1% of the cells had at least one Whi3-3GFP super-assembly away from the ER after 3 h of pheromone treatment, this value dropped to 27.7% ± 10.7%, 20.0% ± 1.7%, and 14.8% ± 4.9% after 4, 6, and 10.5 h of pheromone treatment, respectively (Figure 1I). We conclude that this differential ER membrane association distinguishes Whi3^{mnem} super-assemblies from the prion form of Sup35.

ER compartmentalization is required for the retention of Whi3^{mnem} and the pheromone refractory state in the mother cell

Because Whi3^{mnem} and [*PSI*$^{+}$] differ in their association with ER membranes, we wondered whether the diffusion barriers present in the ER membrane at the yeast bud neck[15] could be the basis for their different modes of inheritance. Diffusion barriers are membrane-specialized domains that limit the diffusion of membrane-associated structures across cellular appendages.[16–18] In budding yeast, diffusion barriers form at the bud neck in the ER membranes and the nuclear envelope.[15,19] Their formation depends on the proteins involved in ceramide biosynthesis,[18,20] including the sphinganine C4-hydroxylase Sur2,[21] and those involved in polarized cell growth, such as the actin-nucleation-promoting factor Bud6[22,23] and the small GTPase Bud1/Rsr1.[24] Thus, we next tested whether the retention of Whi3^{mnem} in the mother cells requires the compartmentalization of ER membranes. We treated the cells expressing Whi3 fused to 3 super-folding GFP in tandem (Whi3-3GFP) with pheromone for 5 h and released them in a pheromone-free medium for 1.5 h to allow the mother cells to produce a bud. The localization of Whi3-3GFP was analyzed in wild-type and barrier-defective cells. Most wild-type, *bud6Δ*, *sur2Δ*, and *bud1Δ* mutant mother cells contained a super-assembly of Whi3^{mnem} (N > 122 cells). However, while only 24.00% ± 6.22% of the wild-type buds had a super-assembly, 62.24% ± 3.85% of the *bud6Δ*, 64.01% ± 3.65% of the *sur2Δ*, and 65.26% ± 4.15% of the *bud1Δ* mutant buds already had at least one (Figures 2A and 2B). These data are consistent with a role for diffusion barriers in the retention of Whi3^{mnem} in the mother cells after escape from pheromone arrest or in the retention of some Whi3 super-assembly regulator.

We next asked whether diffusion barriers are required for the retention of the pheromone refractory state in the mother cell. We exposed haploid *MAT***a** cells to pheromone, as reported.[8] All wild-type cells initially responded to pheromone (7 nM), and 90.5% of the cells escaped pheromone arrest (N = 279 cells) with an average timing of 7.35 ± 3.00 h (Figures 3A and 3B). We previously found that roughly 90% of the daughter cells from the mothers cells that have escaped pheromone arrest shmoo in response to pheromone.[8] Separating data depending on whether the daughter cells were the first or subsequent daughter cells after escape from pheromone arrest, we observed that nearly 50% of the first daughter cells fail to respond to pheromone after birth; however, this number drops to 14.2%,13.3%, 6.9%, and 4.4% for the subsequent 2nd, 3rd, 4th, and 5th daughter cells (Figure 3C).

To assess whether the confinement of the pheromone refractory state to the mother cell is dependent on the presence of diffusion barriers, we tested *sur2Δ*, *bud6Δ*, and *bud1Δ* mutant cells. For reasons that remain unknown, *sur2Δ* mutant cells escaped from pheromone arrest earlier than wild-type cells (5.9 ±2.0 h; Figures 3A and 3B). These mother cells maintained

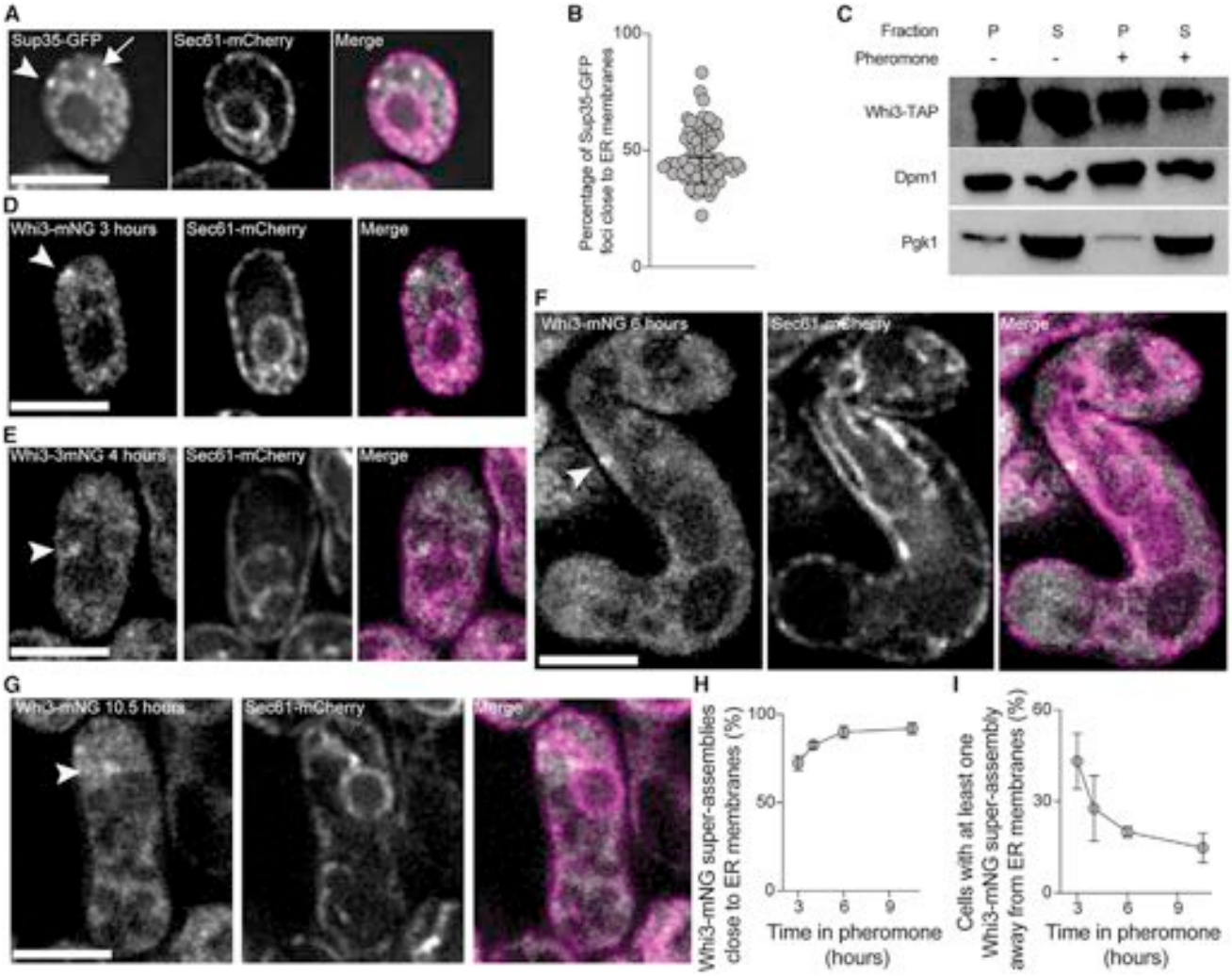

Figure 1. Sup35 prion foci are not closely linked to ER membranes, whereas Whi3 super-assemblies are

(A) Single focal plane images of [*PSI*$^{+}$] cells expressing Sup35-GFP and Sec61-mCherry.

(B) Percentage of Sup35 foci close to ER membranes (1,180 foci analyzed from 90 cells of three independent clones, mean ± SD is presented).

(C) Western blot analysis of Whi3-TAP, an ER marker (Dpm1), and a soluble marker (Pgk1) in the microsome fraction (P, pellet) or the soluble fraction (S, supernatant).

(D and E) (D) Single focal plane images of cells expressing Whi3-mNG and Sec61-mCherry exposed to pheromone for 3 h, (E) 4 h.

(F and G) (F) Single focal plane images of cells expressing Whi3-mNG and Sec61-mCherry exposed to pheromone for 5 h, released in a pheromone-free medium, and then imaged at 6 h and (G) 10.5 h after initial exposure to pheromone.

(H) Percentage of Whi3-mNG super-assemblies close to ER membranes (3 independent clones, >300 super-assemblies from >153 cells were analyzed, mean ± SD are presented).

(I) Percentage of cells with at least one Whi3-mNG super-assembly away from ER membranes (3 independent clones, >300 super-assemblies from >153 cells were analyzed, mean ± SD are presented). Scale bars: 5 μm in (A) and (C–F).

the pheromone refractory state as efficiently as wild-type cells and did not shmoo again. However, the fraction of *sur2Δ* daughter cells that failed to shmoo after separating from their mother cell was increased 1.5 (77.9%)- and 2.8 (40.4%)-fold for the 1st and 2nd daughters, respectively (Figure 3C, p values compared with wild type 0.0004 and 0.0005, two-way ANOVA with Dunnett's multicomparisons test). The *bud6Δ* mutant cells responded to pheromone in a manner similar to that of wild-type cells but escaped pheromone arrest slightly later (Figures 3A and 3B). An increased fraction of *bud6Δ* mutant daughter cells inherited the pheromone refractory state, compared with wild-type cells (Figure 3C). The *bud1Δ* mutant cells showed a similar phenotype (Figures 3A–3C). Supporting the idea that the inheritance of the pheromone refractory state depended on the formation of Whi3 super-assemblies, deleting the Q-rich domain of Whi3, which facilitates the formation of super-assemblies, impaired the inheritance of the refractory state by the daughter cells upon barrier removal. Indeed, most daughter cells of the *WHI3-ΔpQ* mutant cells shmooed upon birth (Figure 3D), and this was not significantly different in the *WHI3-ΔpQ bud6Δ* and *WHI3-ΔpQ bud1Δ* double mutant cells. These results indicate that diffusion barriers facilitate the

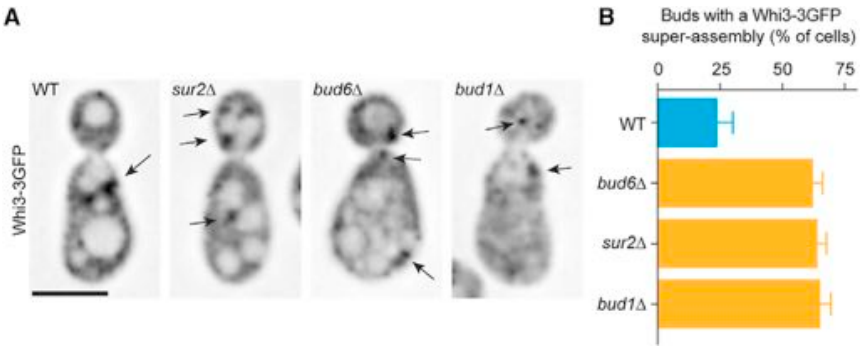

Figure 2. Whi3-3GFP super-assemblies form in the buds of mutants with a weak diffusion barrier

(A) Single focal plane images of Whi3-3GFP expressing cells. Scale bars, 5 μm.

(B) Quantification of buds with a detectable Whi3-3GFP super-assembly (N = 122 cells, 148 cells, 180 cells, and 165 cells for WT, *bud6Δ*, *sur2Δ*, and *bud1Δ* cells, respectively). Results from *bud6Δ*, *sur2Δ*, and *bud1Δ* are significantly different from WT ($p < 0.0001$, one-way ANOVA).

confinement of the pheromone refractory state to the mother cell.

To determine whether the barrier retains Whi3^{mnem} itself or rather a factor regulating the formation of Whi3 super-assembly, we next focused on whether the *bud6Δ, sur2Δ*, or *bud1Δ* mutations affected the timing of the escape of the shmooing daughter cells. We reasoned that these daughter cells may escape faster if they inherit the factors promoting escape from the pheromone arrest formed in the mother cell or if Whi3 condensation is facilitated. However, we did not detect any general effect on the timing of the daughter cells' escape in these mutants (Figure 3E), except that similar to mother cells, the *sur2Δ* daughter cells escaped pheromone arrest faster and *bud6Δ* cells escaped later than wild-type cells. To further characterize the inheritance of the pheromone refractory state in diffusion barrier mutant cells, we exposed cells to pheromone for 3 h and then removed pheromone for 2.5 h to obtain daughter cells that were never exposed to pheromone but were born from cells previously exposed to pheromone. We next reapplied pheromone for the remaining 10.5 h and asked whether the daughter cells shmooed or not. We observed that 11.1% ± 9.9% of the wild-type daughter cells were refractory to pheromone after the second pheromone pulse (Figure 3F). Remarkably, more *sur2Δ*, *bud6Δ*, and *bud1Δ* daughter cells kept on budding (46.5% ± 13.7%, 63.3% ± 23.6%, and 55.5% ± 2.3%, respectively). Thus, the inheritance of the pheromone refractory state by the daughter cells of diffusion barrier mutant cells does not require exposure to pheromone. These data suggest that these cells directly inherit the determinants of the refractory state, such as Whi3^{mnem}, rather than an increased ability to escape.

Finally, we assessed whether forcing the partition of Whi3 in the bud despite functional diffusion barriers is sufficient to pass the pheromone refractory state on to the daughter cells. We, therefore, anchored Whi3 to the spindle pole body (SPB). Indeed, during each cell division, one of the two spindle pole bodies was inherited by the daughter cell. We fused the GFP-binding protein (GBP) and the red fluorescent protein (RFP) to the SPB component Spc42 and coexpressed this fusion protein (Spc42-GBP) with Whi3-GFP. Consistent with the GFP- and GBP-mediated synthetic physical interaction,[25] Whi3-GFP was recruited to SPBs in these cells (Figure 3G). Upon pheromone exposure and escape, less than 35.0% of the daughter cells of cells expressing Whi3-GFP or Spc42-GBP alone inherited the refractory state of their mother; however, this proportion increased up to 70.3% in the cells coexpressing both proteins (Figure 3H). The expression of Spc42-GBP ± Whi3-GFP did not affect the timing of the escape of the mother cells, indicating that the kinetics of pheromone response and escape were unaffected (Figure S1). We conclude that forcing Whi3^{mnem} into the bud is sufficient for conferring the refractory state to the daughter cells.

Altogether, we conclude that the cortical ER diffusion barrier contributes to the confinement of the pheromone refractory state as well as Whi3^{mnem} to the mother cell during cell division. This is consistent with Whi3^{mnem} associating with ER membranes and the formation of Whi3^{mnem} in the bud being restricted by the diffusion barrier (Figures 1 and 3). Importantly, in cells lacking a functional barrier, the inheritance of the refractory state by the daughter cells does not take place at the cost of the mother cell losing the pheromone refractory state.

ER compartmentalization is not required for prion induction and curing

Together, these data suggested that the confinement of a prion-like state to the mother cell might require its attachment to the ER membrane and the compartmentalization of that membrane. To test this idea further, we next asked whether the ER-membrane diffusion barriers play any role in [*PSI*$^+$] prion induction or curing. Using a copy of the GFP gene that contains in-frame stop codons (GFP^{STOP}) as a reporter for readthrough frequency in [*PSI*$^+$] cells, we previously observed that the farnesylation of the Hsp40 co-chaperone Ydj1 dampens premature stop codon readthrough.[14] Using flow cytometry, no change in green-fluorescence intensity was observed between wild-type and *sur2Δ* mutant [*PSI*$^+$] cells expressing the GFP^{STOP} allele (Figure 4A). Likewise, no significant difference ($p = 0.5204$, t test) in the [*PSI*$^+$] appearance frequency was observed between the wild-type and *sur2Δ* mutant strains (Figure 4B), using the *ade1-14* (white [*PSI*$^+$])/(red [*psi*$^-$]) colonies assay.[26] The dynamics of [*PSI*$^+$] curing by guanidine hydrochloride (GuHCl, 3 mM) were also very similar between these cells (Figure 4C, white/red colony assay). Since the growth of wild-type and *sur2Δ* strains were equivalent (Figure 4D), we concluded that the loss of [*PSI*$^+$] was indistinguishable. Moreover, GFP^{stop} intensity decreased comparably in the wild-type and *sur2Δ* cells treated with 0.1 and 1 mM GuHCl, demonstrating that the stop codon readthrough was quantitively measured (Figure 4A). Altogether, these data establish that ER compartmentalization at the bud neck does not affect the inheritance of Sup35 seeds during cell division, consistent with Sup35 aggregates being away from ER membranes.

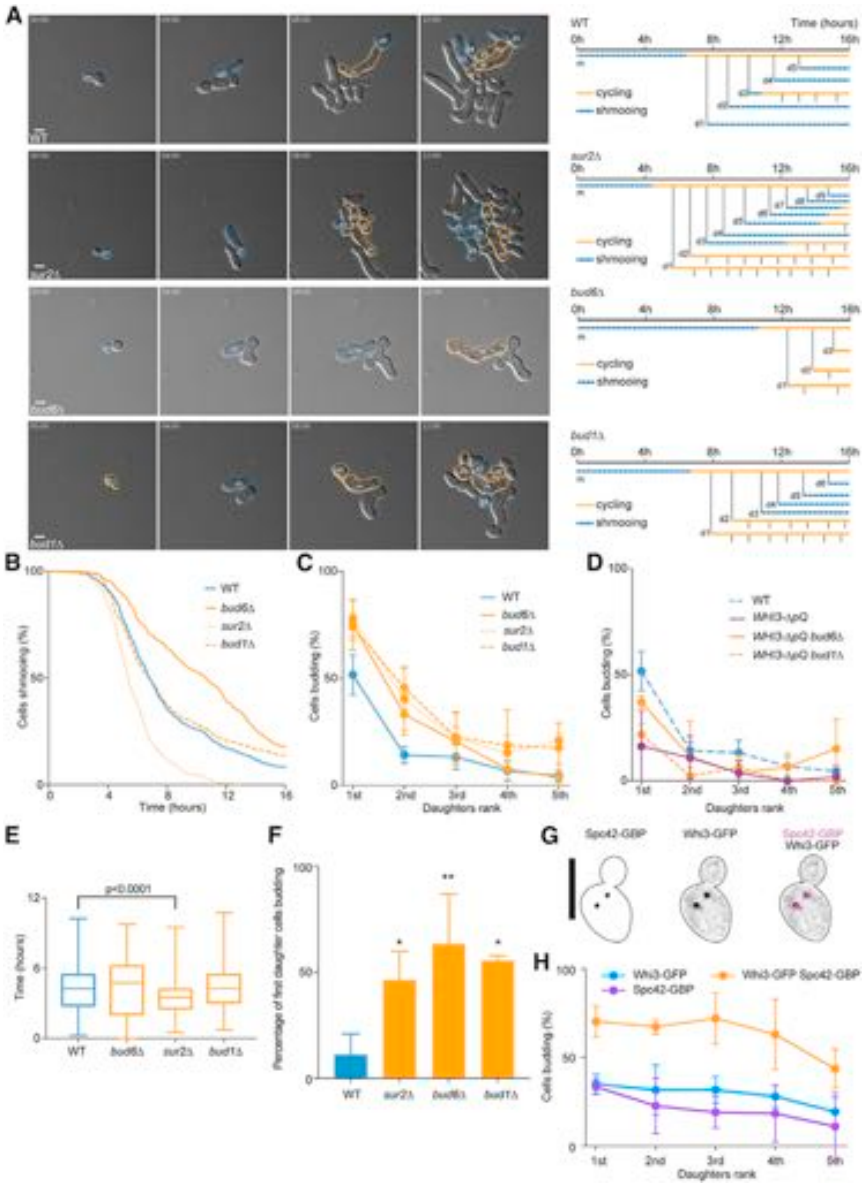

Figure 3. The ER diffusion barrier prevents the daughter cells from inheriting the pheromone refractory state

(A) Escape of a WT, a *bud6Δ*, a *sur2Δ*, and a *bud1Δ* cell exposed to 7 nM pheromone. Scale bars, 5 μm.

(B) Percentage of initial cells still shmooing after the indicated time (N > 154 cells).

(C and D) Percentage of the daughter cells budding immediately after separation from the mother cell (N > 128 cells, N > 121 cells, N > 111 cells, N > 88 cells, and N > 59 cells for the 1st, 2nd, 3rd, 4th, and 5th daughter cells, respectively). Mean ± SD are presented.

(E) Box plot of the timing of escape of the daughter cells of indicated genotypes that are shmooing (N > 81 cells).

(F) Percentage of the 1st daughter cells budding after a second pulse of pheromone (N > 27 cells). Mean ± SD are presented.

(G) Localization of Whi3-GFP and Spc42(-RFP)-GBP. Scale bars, 5 μm.

(H) Percentage of the daughter cells budding immediately after separation from the mother cell (N > 81 cells, N > 50 cells, N > 40 cells, N > 28 cells, and N > 19 cells for the 1st, 2nd, 3rd, 4th, and 5th daughter, respectively). Mean ± SD are presented. See also Figure S1.

Cells lacking diffusion barriers can acquire a stable pheromone refractory trait

We next tested whether the inheritance of the pheromone refractory state could be detected by growth assays on solid media containing pheromone. On medium containing low concentration of pheromone (10 nM), wild-type cells grew slowly and cells that hardly escape pheromone arrest (*WHI3-ΔpQ*) grew very poorly (Figure 5A). Both strains grew similarly on a medium lacking pheromone. This reflects the fact that the *WHI3-ΔpQ* mutant cells shmoo for a long time before resuming cell division, often not even escaping pheromone-induced cell-cycle arrest. In contrast, wild-type cells produce daughter cells earlier. Several *bud1Δ*, *bud6Δ*, and *sur2Δ* mutant strains grew as slowly as wild-type cells; however, others (bottom lane in Figure 5A) grew much better on pheromone-containing plates, even at a high pheromone concentration (0.6 μM, Figure 5A). At such a high concentration of pheromone, cells normally do not escape pheromone arrest, suggesting that these colonies had acquired a strong resistance to pheromone. Indeed, the resistance to pheromone was maintained even after several rounds of streaking; we termed these isolates as constitutive escapers (CE). Remarkably, our observation suggested that CE formed more frequently in barrier mutants than in wild-type strains.

To measure CE frequency, we plated independent clones on rich media with or without pheromone (0.6 μM, Figures 5A and 5B). Frequency of CE was highly variable between individual clones of wild-type strains (1.1×10^{-7}–5.3×10^{-2}) with a median of 1.4×10^{-5} cells. The phenotypic mutation rate for sterile mutants was measured in a *bar1Δ* background at 3.1×10^{-6}/genome/generation.[27] The CE phenotype was also variable in *sur2Δ* clones, but the median (4.3×10^{-5}) was significantly increased 3 times compared with wild type (Figure 5B). In *bud6Δ* and *bud1Δ* mutant cells, frequencies varied between clones and the median frequency was significantly increased 6 times (8.3×10^{-5}) and 3.5 times (4.8×10^{-5}), respectively, compared with wild type. Standardizing the variances, a linear model describing the means of each strain showed a significant difference between wild-type and diffusion barrier mutants (Figure 5C, ANOVA $p < 2e{-}16$). Therefore, disruption of the diffusion barrier increases the frequency at which a mitotically stable state of pheromone resistance is established beyond the rate expected by mutation. These data also indicated that the CE trait might be of epigenetic nature, which may have been caused by a prion.

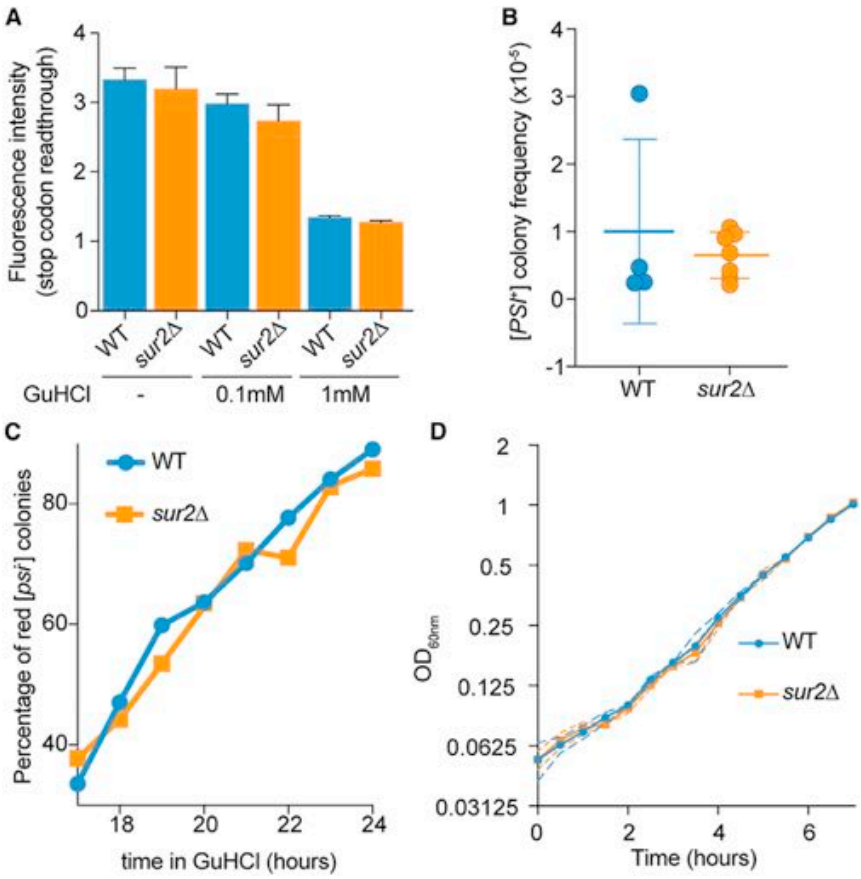

Figure 4. ER compartmentalization by a lateral membrane diffusion barrier is not required for prion induction and curing

(A) Fluorescence intensity measured by flow cytometer of the [*PSI*$^+$] WT and [*PSI*$^+$] *sur2Δ* cells treated or not treated with 0.1 and 1 mM GuHCl. (B and C) (B) Frequency of *de novo* [*PSI*$^+$] appearance and (C) percentage of cells cured of [*PSI*$^+$] over time. Graphs (A) and (B) display mean ± SD. (D) Growth curves of WT and *sur2Δ* strains assessed by OD_{600nm}.

Prions segregate in a non-Mendelian manner, often passed on to the four meiotic products. We, therefore, analyzed how pheromone resistance segregated during meiosis. Most of the backcrossed CE displayed a non-Mendelian inheritance of pheromone resistance, consistent with a prion hypothesis (Figure S2). To further test this hypothesis, we tried to cure the CE strains. Except for one isolate (CE1$^{sur2\Delta}$), the inhibition of Hsp104, Hsp90, or Hsp70 did not cure the CE phenotype (Figure S2). Therefore, the CE trait is largely insensitive to classical prion-curing agents. Thus, our data are consistent with the CE trait being due to a non-Mendelian agent, possibly a nonclassical prion.

We next rationalized that Whi3 may adopt a prion form in a subfraction of the CE. Accordingly, we noticed that some CE isolates formed smaller cells than wild-type cells. While the wild-type and *sur2Δ* parental strains had comparable cell size (5.6 μm, Figure 5D), the CE$^{sur2\Delta}$ clones appeared in mainly two categories, displaying either small or large cell sizes. Remarkably, the small-cell-sized CE$^{sur2\Delta}$ clones were comparable in size with *whi3Δ* cells (±*sur2Δ*, Figure 5D).

To test whether Whi3 may be in a prion form in small CE, we monitored the cell size and the localization of Whi3-GFP in 20 CE$^{sur2\Delta}$ isolates. In the parental *sur2Δ* mutant strain, Whi3-GFP localized diffusely throughout the cytoplasm and to a few granules ([8,11] and Figure 5E). In the small-cell-sized CE$^{sur2\Delta}$ isolates, Whi3 localized both diffusely throughout the cytoplasm and to brighter foci that were substantially bigger and more intense than the granules shown by the parental strain. Large-cell-sized CE clones contained less of such foci (Figures 5E and 5F). Remarkably, these bright foci localized both to the mother and the bud compartments of the dividing cells. Therefore, in small-cell-sized CE$^{sur2\Delta}$ isolates, Whi3 tends to adopt a localization reminiscent to that of Sup35 in its [*PSI*$^+$] form, thus supporting the idea that it is in a prion-like form.

Because Sup35 in its [*PSI*$^+$] form was not strongly associated with ER membranes but Whi3^{mnem} super-assemblies were, we wondered whether Whi3 in CE was still associated with ER membranes. 60.3% of the Whi3-mNG foci were close to ER membranes in CE$^{bud6\Delta}$ cells (Figures 5G and 5H). By comparison, the granules of non-CE *bud6Δ* cells and Whi3^{mnem} super-assemblies were more tightly associated to ER membranes (88.2%, Figures 1C–1G, 5G, and 5H). Thus, the localization of Whi3 in CE cells is reminiscent of that of Sup35 in [*PSI*$^+$] cells in terms of shape (bright foci) and association to ER membranes.

Altogether, these results establish that the disruption of the diffusion barrier increases the appearance of CE and that many CE form small cells with a fraction of Whi3 in bright foci. Supporting the notion that the conversion of Whi3 to a prion form facilitates the formation of CE, we observed that the frequency of CE was lower in strains expressing the *WHI3-ΔpQ* mutation than in wild-type strains (Figures 5B and 5C, $p < 0.0008$ from Figure 5C). Furthermore, this frequency was not enhanced by inactivating the diffusion barrier (*WHI3-ΔpQ bud1Δ*), emphasizing the role of the Whi3 polyQ domain in promoting CE formation when diffusion barriers are impaired. Conversely, adding a second copy of *WHI3* increased the frequency of CE formation 2.4-fold (Figure 5I, $p = 0.016$).

However, the CE trait was not solely due to the conversion of Whi3 into a prion because nearly half of the CE clones did not form small cells and did not contain an increased frequency of Whi3 aggregates. In addition, the *WHI3-ΔpQ* allele did not fully abolish CE formation (Figure 5B) and deleting the *WHI3* gene in CE did not cure them. Our data suggest that the CE trait is due to the conversion of at least two epigenetic switches, one that involves Whi3 inactivation through its conversion to a propagating form, and a second one, possibly another prion. To test whether the inactivation of Whi3 promotes the formation of the CE trait,

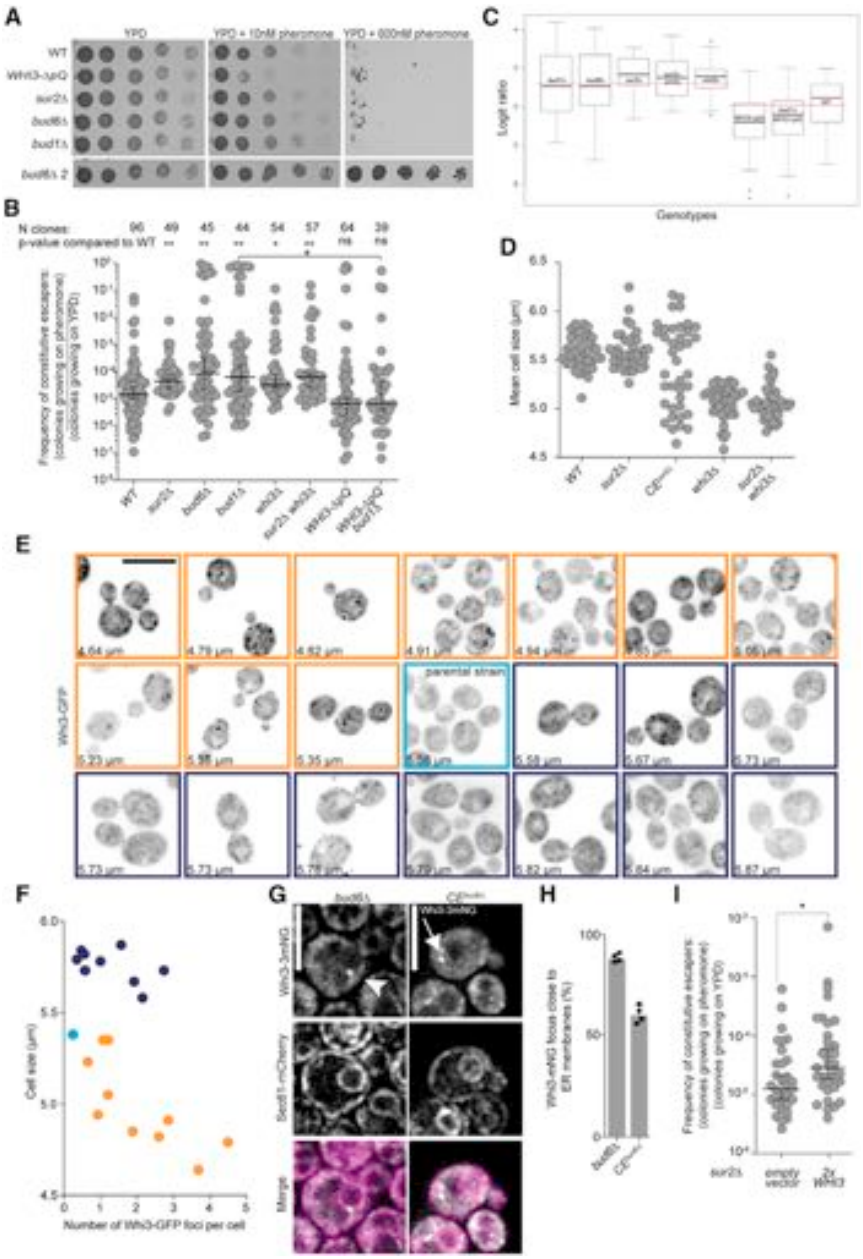

Figure 5. A novel epigenetic phenotype, constitutive escapers

(A) Serial 1/10 dilutions of exponentially growing cultures of indicated strains spotted on a YPD solid medium (left) or YPD containing pheromone (10 nM middle and 600 nM right). The bottom panel shows another *bud6Δ* independent clone with a high frequency of CE.

(B) Frequency of appearance of CE in the indicated genotypes (median with 95% confidence interval, N > 37 clones for each, Dunn's multiple comparisons test was used to determine significance).

(C) Distribution of the logit transformed ratios (R) for each genotype.

(D) Cell-size distributions of individual clones or CE isolates of indicated strains (N > 39 clones for each).

(E) Maximal projection images of the *sur2Δ* cells expressing Whi3-GFP from 20 CE isolates and the parental strain. Isolates are in the order of the mean cell size from the smallest (orange-framed are smaller than the blue-framed parental strain) to the largest (purple are larger than the parental strain). Scale bars, 5 μm.

(F) Number of Whi3-GFP bright foci per cell in the 20 CE isolates and the parental strain as a function of cell size.

(G) Single focal plane images of *bud6Δ* cells (top) and $CE^{bud6\Delta}$ cells (bottom) expressing Whi3-mNG and Sec61-mCherry. Scale bars, 5 μm.

(H) Percentage of Whi3-mNG granules (*bud6Δ*) and foci ($CE^{bud6\Delta}$) localizing close to ER membranes (4 clones or isolates, 527 granules, and 359 foci in 200 cells were analyzed, mean ± SD are presented). The arrow points at a focus away from the ER and the arrowhead points at focus close to the ER.

(I) Frequency of appearance of CE in the indicated genotypes (median with 95% confidence interval, N > 33 clones for each, Mann-Whitney test was used to determine significance). See also Figures S2, S3, and S7 and Methods S1.

we measured the frequency of CE in *whi3Δ* mutant strains. The deletion of *WHI3* increased the frequency of CE compared with wild-type (2.5 times, 3.3×10^{-5}) and even more in *sur2Δ* strains (4.6 times, 6.2×10^{-5}, Figure 5B). These results support a mechanism for CE formation that involves the inactivation of Whi3 and possibly other prions.

To further evaluate the role of Whi3 in CE formation, we obtained small CEs, deleted *WHI3-GFP*, and reintroduced *WHI3-GFP* after >50 generations of growth without *WHI3* expression. Of the 4 CEs evaluated, 3 were still growing on pheromone. The fourth isolate resumed shmooing in response to pheromone (Figure S3) and displayed a localization of Whi3-GFP that was close to wild type and cell size was restored (Figure S3), suggesting that in this case, a cycle of deletion-reintroduction of *WHI3* did cure the CE phenotype or that another uncontrolled event occurred during the >50 generations of growth. Thus, it seems that Whi3 itself has the potential to behave as a prion. Additional proteins may show a similar behavior, contributing to the phenotype in some CE isolates together or in place of Whi3.

Altogether, our data indicate that most of the CE that emerged from the cells lacking a diffusion barrier at the bud neck are due to a non-Mendelian factor and suggest that the conversion of Whi3 to a prion form contributes to their formation.

The prion-like domain of Whi3 can adopt a self-templating conformation

Since our data suggested that Whi3 can switch to a self-templating conformation, we wondered whether this property could be recapitulated *in vitro*. Therefore, we synthesized Whi3's Q-rich prion-like domain ($Whi3^{polyQ}$, Figure 6A) and tested its ability to form assemblies *in vitro*. $Whi3^{polyQ}$ was

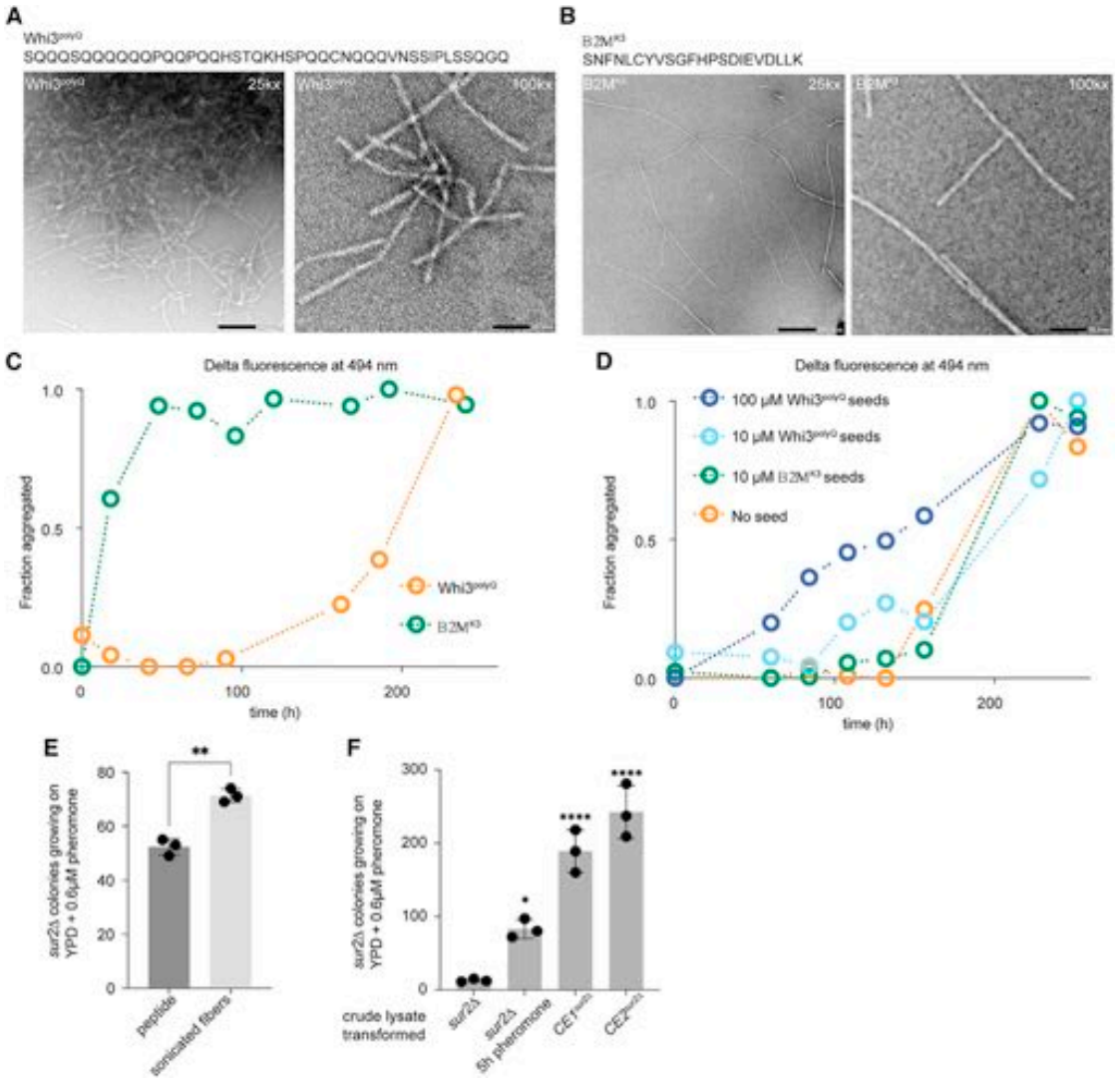

Figure 6. The polyQ domain of Whi3 has a self-templating activity

(A) Sequence of the Whi3^{polyQ} peptide and fibers observed after 7 days of growth.

(B) Sequence of the B2M^{K3} peptide and fibers observed after 7 days of growth. Scale bars: 200 nm for 25 kx magnification and 50 nm for 100 kx magnification.

(C) The fibrillar growth, monitored by bisANS, of B2M^{K3} (green) and Whi3^{polyQ} (orange) fibers is shown.

(D) BisANS fluorescence monitoring of fibrillar growth for Whi3^{polyQ} without (orange), or with B2M^{K3} seeds (green) and Whi3^{polyQ} seeds at two different concentrations (light and dark blue for 10 and 100 µM, respectively).

(E) Number of colonies growing on YPD + pheromone (0.6 µM) after transformation with either the native Whi3^{polyQ} peptide or sonicated fibers of Whi3^{polyQ}. Mean ± SD are presented. ** denotes a p value < 0.01 using an unpaired t test.

(F) Number of colonies growing on YPD + pheromone (0.6 µM) after transformation with a crude lysate from *sur2Δ* cells ± pheromone treatment for 5 h or CE$^{sur2\Delta}$ cells.Mean ± SD are presented. p values: * < 0.05, **** < 0.0001 using an ANOVA. See also Figures S4, S5, and S6 and Tables S1, S2, S3, S4, S5, and S6.

incubated for several days at pH 7.4, 30°C. Electron microscopy analysis showed that Whi3^{polyQ} forms amyloid fibers under these conditions (Figure 6A). These assemblies were generally shorter and thicker (7.45 ± 0.8 nm versus 5.11 ± 0.61 nm) than those produced by an amyloidogenic fragment of human β_2-microglobulin, B2M^{K3},[28,29] which was used here as a control (Figure 6B; Table S1). Moreover, the Whi3^{polyQ} and B2M^{K3} fibrils interact with the fluorogenic dyes thioflavin T (ThT) and 4,4′-dianilino-1,1′-binaphthyl-5,5′-disulfonic acid (bisANS) differently (Figure S4), suggesting distinct molecular structures.

Using bisANS as a reporter, fiber growth was monitored by fluorescence spectroscopy (Figures 6C and 6D). The assembly of Whi3^{polyQ} was characterized by a longer lag phase than that of B2M^{K3}, but once initiated, the fluorescence increased very rapidly (Figure 6C), consistent with nucleation being rate-limiting. The lag phase could be substantially reduced by adding Whi3^{polyQ} seeds, which was generated by sonicating preformed Whi3^{polyQ} fibers, to the samples. In contrast, B2M^{K3} seeds had no effect on the growth of Whi3^{polyQ} fibrils (Figure 6D). These data demonstrate that, at least *in vitro*, the Whi3 Q-rich domain displays a self-templating activity.

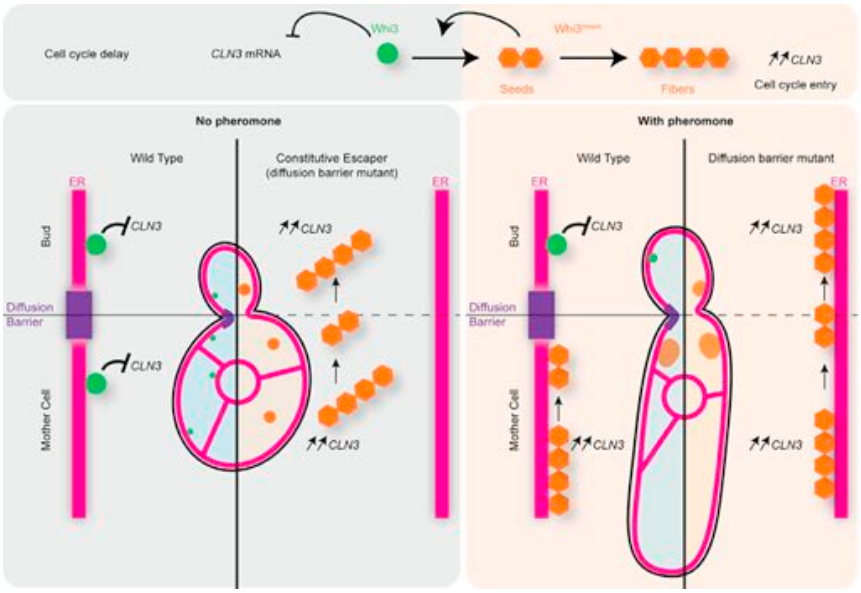

Figure 7. Schematic of Whi3 behavior in different conditions (±pheromone) and genotypes (±diffusion barrier)

To test whether the *in vitro* assembly of Whi3^{polyQ} is related to the CE phenotype, we transformed the native Whi3^{polyQ} peptide or sonicated fibers of Whi3^{polyQ} into *sur2Δ* cells and plated them on pheromone-containing plates (0.6 μM). We observed a 1.4-fold increase in the colonies growing on pheromone when the sonicated fibers were transformed compared with the native peptide (Figure 6E; p = 0.0011, unpaired t test). We next assessed whether *sur2Δ* cells could also be transformed by crude lysates of CE to induce more CE. The transformation of a crude lysate from *sur2Δ* cells treated with pheromone for 5 h lead to a 6.6-fold increase in the number of colonies growing on yeast extract peptone dextrose (YPD) + pheromone (0.6 μM) compared with the transformation of crude lysates obtained from exponentially growing *sur2Δ* cells (Figure 6F). This increase was more than doubled further when the crude lysates from CE^{sur2Δ} were transformed (Figure 6F). Interestingly, we did not observe such an increase in CE frequency when transforming a wild-type strain (Figure S5). Altogether, our data suggest that both during escape from pheromone arrest and in CE, Whi3 adopts a self-templating conformation that can propagate to the daughter cells in diffusion barrier defective cells.

DISCUSSION

Cells can preserve the memories of some previous adaptations to tune their response to the environment. The ability of a self-templating prion-like protein like Whi3^{mnem} to encode such memory is a case in point. A remarkable characteristic of Whi3^{mnem} is its confinement to the mother cell that experienced deceptive courtship. This spatially restricted behavior is reminiscent of the role of synapses in neuronal memory, where the activated synapses—but not the neighboring ones—are potentiated in the long term. Strikingly, one of the molecular events that supports long-term potentiation is a functional switch of the prion-like protein CPEB/Orb2 in the postsynaptic spines.[30–34] Similar to Whi3, CPEB/Orb2 is an RNA-binding protein that regulates the translation of target mRNAs. Furthermore, the spatial restriction of spine potentiation relies at least in part on the presence of a membrane diffusion barrier at the neck separating the spine from the dendritic shaft.[35–37] We propose that the mechanisms of mnemon-based cellular memory are similar in yeast and metazoans, indicating a long evolutionary history.

The self-templating conformational change of prion-like proteins is a powerful mechanism to sustain cellular memory over a long period of time. Indeed, the seeds obtained from Whi3^{polyQ} fibrils nucleate fibril formation. Thus, the presence of some seeds in the cell may template the conformational change and fibril assembly of the newly made Whi3. Consequently, this conformational change may last much longer than the lifetime of individual proteins. In fact, when one of the two prion-like domains of Whi3 is removed, the pheromone refractory state is not firmly established and cells eventually revert to a shmooing phase.[8] Furthermore, the fact that Whi3^{mnem} may propagate as a prion once confinement is lifted provides strong support to the notion that Whi3^{mnem} undergoes events of a self-templated maintenance. Similarly, CPEB self-templates amyloid formation, providing a mechanism for the long-term potentiation of the activated synapse.[33] Orb2 in *Drosophila* is required for a long-term potentiation, but not for short-term memory, indicating that cells use prion-like proteins to stabilize structurally encoded memory.[30] In both cases, memory is encoded by a fibril-forming protein that promotes mRNA translation upon conversion, releasing the *CLN3* mRNA from translational inhibition for Whi3 and activating the expression of long-term potentiation factors for CPEB. Therefore, the prion-like conversion and self-perpetuation of such mRNA binding proteins emerge as key mechanisms for encoding long-term memories at the cellular level.

The conundrum of a prion-based mechanism for cellular memory is that the self-templating activity of these proteins bears the potential of converting the entire pool of molecules in the cell and beyond. This would, in principle, preclude such mechanisms from remaining spatially defined, such as being restricted to activated spines or yeast mother cells. Here, we show that self-templating Whi3^{mnem} is confined to the mother cell and that this confinement correlates with the close association of Whi3^{mnem} with compartmentalized ER membranes (see Figure 7). Indeed, when the barriers are disrupted, the mother cells start to share Whi3^{mnem} and the refractory state with their daughter cells. Remarkably, the main super-assembly remains in the mother cell, suggesting that daughter cells receive seeds of Whi3^{mnem}. The propagation of Whi3^{mnem} is most prevalent during the first divisions following escape from pheromone arrest, suggesting that the pool of diffusible Whi3^{mnem} seeds is limited. We propose that after this, the super-assemblies mature to a form that no

longer generate seeds. In the CE isolates, Whi3 might adopt a conformation that keeps on generating seeds. A diversity of Whi3 prion "strains" would explain why only a fraction of cells turns into CE and why distinct CE show different cell sizes. Thus, our data emphasize the importance of confinement for at least Whi3^{mnem} and restricting its infectious potential in a prion-like manner.

The prion strain of Whi3 seems to share most properties of its mnemon counterparts, except for a reduced ability to associate with the ER membrane. As we show, this is also the case for Sup35 in its [*PSI*$^{+}$] prion form. Thus, membrane association might be a distinctive feature of mnemons. Together, our studies suggest that confinement may play an important role not only in preventing the propagation of the self-templating entities but also in constraining which self-templating strains are formed.

The distinction between prions and mnemons points to different cellular strategies selected to either encode collective memory which are passed to the entire yeast colony, for example, by prions[38–42] or individual memory, restricted to the cell that experienced the memorized event. The selection of mechanisms (prions or mnemons) may relate to which strategy would be more efficient. While the adaptive advantages of prions have been discussed,[43–45] mnemons provide an individualized mechanism for single cells to adapt to a signal and keep the opportunity for their progeny to remain naive. The value of such a strategy is evident in the case of mating because the daughter cells might be better placed relative to a potential partner to allow for a successful mating; however, in reverse, the stable propagation of the refractory state has the disadvantage of turning a single deceptive encounter into the sterility of the entire subsequent colony.

The similarities between the dendritic spine neck and the yeast bud neck[35–37] suggest that lateral membrane diffusion barriers could contribute to dendritic spine individualization through the compartmentalization of mnemons in the activated spines. Such a model is supported by CPEB linkage to membranes in oocytes[46] and Orb2 amyloids being enriched in synaptic membrane fractions.[47] Thus, we suggest that budding yeast might provide an interesting model for studying some of the mechanisms of spine function and potentiation.

Finally, we believe that our results are relevant to pathological situations such as neurodegenerative diseases. If aging or genetic mutations were to favor unleashing mnemons from their prion potential, allowing them to spread to the entire cell and from one cell to another, this could promote the emergence of phenotypes very similar to those observed in neurodegenerative diseases such as Parkinson and Alzheimer diseases. Age may, for example, allow the emergence of propagating strains or affect the strength of confinement. Indeed, the compartmentalization of ER membranes is lost in neural stem cells of aged mice.[48] Thus, we propose that in some cases, neurodegenerative diseases may be strain and or confinement diseases.

STAR★METHODS

Detailed methods are provided in the online version of this paper and include the following:

SUPPLEMENTAL INFORMATION

Supplemental information can be found online at https://doi.org/10.1016/j.cub.2022.01.002.

ACKNOWLEDGMENTS

We would like to thank the Thorpe group for their help with the GFP/GBP experiments and feedback. We would also like to thank the whole McMurray group for their constructive feedback posted on Pubpeer. This work was supported by a Biotechnology and Biological Sciences Research Council project grant (BB/S001204/1) to F.C. and H.P.O.; QMUL to F.C., Y.L., and H.P.O.; MUSE funding to F.C.; the Academy of Finland (317038) and Sigrid Jusélius Foundation to J.S.; and the European Research Council (BarrAge 250278) and ETH Zurich to D.H., J.S., F.C., and Y.B.

AUTHOR CONTRIBUTIONS

F.C., Y.B., and D.H. conceived the study. Y.L., H.P.O., M.G., I.P., J.S., R.H., and F.C. performed experiments and analyzed the data. R.A.N. analyzed the constitutive escapers data. F.C. wrote the manuscript with input from Y.B. and edits from all the authors.

DECLARATION OF INTERESTS

The authors declare no competing interests.

INCLUSION AND DIVERSITY

One or more of the authors of this paper self-identify as an underrepresented ethnic minority in science.

Received: September 7, 2020
Revised: October 19, 2021
Accepted: January 4, 2022
Published: January 26, 2022

REFERENCES

1. Hou, F., Sun, L., Zheng, H., Skaug, B., Jiang, Q.-X., and Chen, Z.J. (2011). MAVS forms functional prion-like aggregates to activate and propagate antiviral innate immune response. Cell *146*, 448–461.
2. Coustou, V., Deleu, C., Saupe, S., and Begueret, J. (1997). The protein product of the het-s heterokaryon incompatibility gene of the fungus Podospora anserina behaves as a prion analog. Proc. Natl. Acad. Sci. USA *94*, 9773–9778.
3. True, H.L., and Lindquist, S.L. (2000). A yeast prion provides a mechanism for genetic variation and phenotypic diversity. Nature *407*, 477–483.
4. Yuan, A.H., and Hochschild, A. (2017). A bacterial global regulator forms a prion. Science *355*, 198–201.
5. Prusiner, S.B. (1982). Novel proteinaceous infectious particles cause scrapie. Science *216*, 136–144.
6. Goedert, M. (2015). NEURODEGENERATION. Alzheimer's and Parkinson's diseases: the prion concept in relation to assembled Aβ, tau, and α-synuclein. Science *349*, 1255555.
7. Suzuki, G., Shimazu, N., and Tanaka, M. (2012). A yeast prion, Mod5, promotes acquired drug resistance and cell survival Under environmental stress. Science *336*, 355–359.
8. Caudron, F., and Barral, Y. (2013). A super-assembly of Whi3 encodes memory of deceptive encounters by single cells during yeast courtship. Cell *155*, 1244–1257.
9. Moore, S.A. (1984). Yeast cells recover from mating pheromone alpha factor-induced division arrest by desensitization in the absence of alpha factor destruction. J. Biol. Chem. *259*, 1004–1010.
10. Alberti, S., Halfmann, R., King, O., Kapila, A., and Lindquist, S. (2009). A systematic survey identifies prions and illuminates sequence features of prionogenic proteins. Cell *137*, 146–158.
11. Garì, E., Volpe, T., Wang, H., Gallego, C., Futcher, B., and Aldea, M. (2001). Whi3 binds the mRNA of the G1 cyclin *CLN3* to modulate cell fate in budding yeast. Genes Dev *15*, 2803–2808.
12. Tuite, M.F. (2016). Remembering the past: a new form of protein-based inheritance. Cell *167*, 302–303.
13. Vergés, E., Colomina, N., Garí, E., Gallego, C., and Aldea, M. (2007). Cyclin *CLN3* is retained at the ER and released by the J chaperone Ydj1 in late G1 to trigger cell cycle entry. Molecular Cell *26*, 649–662.
14. Saarikangas, J., Caudron, F., Prasad, R., Moreno, D.F., Bolognesi, A., Aldea, M., and Barral, Y. (2017). Compartmentalization of ER-bound chaperone confines protein deposit formation to the aging yeast cell. Curr. Biol. *27*, 773–783.
15. Luedeke, C., Frei, S.B., Sbalzarini, I., Schwarz, H., Spang, A., and Barral, Y. (2005). Septin-dependent compartmentalization of the endoplasmic reticulum during yeast polarized growth. J. Cell Biol. *169*, 897–908.
16. Caudron, F., and Barral, Y. (2009). Septins and the lateral compartmentalization of eukaryotic membranes. Dev. Cell *16*, 493–506.
17. Saarikangas, J., and Barral, Y. (2011). The emerging functions of septins in metazoans. EMBO Rep *12*, 1118–1126.
18. Prasad, R., Sliwa-Gonzalez, A., and Barral, Y. (2020). Mapping bilayer thickness in the ER membrane. Sci. Adv. *6*, eaba5130.
19. Shcheprova, Z., Baldi, S., Frei, S.B., Gonnet, G., and Barral, Y. (2008). A mechanism for asymmetric segregation of age during yeast budding. Nature *454*, 728–734.
20. Megyeri, M., Prasad, R., Volpert, G., Sliwa-Gonzalez, A., Haribowo, A.G., Aguilera-Romero, A., Riezman, H., Barral, Y., Futerman, A.H., and Schuldiner, M. (2019). Yeast ceramide synthases, Lag1 and Lac1, have distinct substrate specificity. J. Cell Sci. *132*, jcs228411.
21. Clay, L., Caudron, F., Denoth-Lippuner, A., Boettcher, B., Buvelot Frei, S., Snapp, E.L., and Barral, Y. (2014). A sphingolipid-dependent diffusion barrier confines ER stress to the yeast mother cell. Elife *3*, e01883.
22. Graziano, B.R., Jonasson, E.M., Pullen, J.G., Gould, C.J., and Goode, B.L. (2013). Ligand-induced activation of a formin-NPF pair leads to collaborative actin nucleation. J. Cell Biol. *201*, 595–611.
23. Graziano, B.R., DuPage, A.G., Michelot, A., Breitsprecher, D., Moseley, J.B., Sagot, I., Blanchoin, L., and Goode, B.L. (2011). Mechanism and cellular function of Bud6 as an actin nucleation-promoting factor. Mol. Biol. Cell *22*, 4016–4028.
24. Bender, A., and Pringle, J.R. (1989). Multicopy suppression of the cdc24 budding defect in yeast by CDC42 and three newly identified genes including the ras-related gene RSR1. Proc. Natl. Acad. Sci. USA *86*, 9976–9980.
25. Ólafsson, G., and Thorpe, P.H. (2015). Synthetic physical interactions map kinetochore regulators and regions sensitive to constitutive Cdc14 localization. Proc. Natl. Acad. Sci. USA *112*, 10413–10418.
26. Eaglestone, S.S., Ruddock, L.W., Cox, B.S., and Tuite, M.F. (2000). Guanidine hydrochloride blocks a critical step in the propagation of the prion-like determinant [*PSI*$^+$] of Saccharomyces cerevisiae. Proc. Natl. Acad. Sci. USA *97*, 240–244.
27. Lang, G.I., and Murray, A.W. (2008). Estimating the per-base-pair mutation rate in the yeast Saccharomyces cerevisiae. Genetics *178*, 67–82.
28. Kozhukh, G.V., Hagihara, Y., Kawakami, T., Hasegawa, K., Naiki, H., and Goto, Y. (2002). Investigation of a peptide responsible for amyloid fibril formation of β2-microglobulin byAchromobacter protease I. J. Biol. Chem. *277*, 1310–1315.
29. Torbeev, V., Grogg, M., Ruiz, J., Boehringer, R., Schirer, A., Hellwig, P., Jeschke, G., and Hilvert, D. (2016). Chiral recognition in amyloid fiber growth. J. Pept. Sci. *22*, 290–304.
30. Keleman, K., Krüttner, S., Alenius, M., and Dickson, B.J. (2007). Function of the Drosophila CPEB protein Orb2 in long-term courtship memory. Nat. Neurosci. *10*, 1587–1593.
31. Li, L., Sanchez, C.P., Slaughter, B.D., Zhao, Y., Khan, M.R., Unruh, J.R., Rubinstein, B., and Si, K. (2016). A putative biochemical engram of long-term memory. Curr. Biol. *26*, 3143–3156.
32. Si, K., Choi, Y.-B., White-Grindley, E., Majumdar, A., and Kandel, E.R. (2010). Aplysia CPEB can form prion-like multimers in sensory neurons that contribute to long-term facilitation. Cell *140*, 421–435.
33. Si, K., Lindquist, S., and Kandel, E.R. (2003). A neuronal isoform of the Aplysia CPEB has prion-like properties. Cell *115*, 879–891.
34. Hervas, R., Rau, M.J., Park, Y., Zhang, W., Murzin, A.G., Fitzpatrick, J.A.J., Scheres, S.H.W., and Si, K. (2020). Cryo-EM structure of a neuronal functional amyloid implicated in memory persistence in *Drosophila*. Science *367*, 1230–1234.
35. Tada, T., Simonetta, A., Batterton, M., Kinoshita, M., Edbauer, D., and Sheng, M. (2007). Role of septin cytoskeleton in spine morphogenesis and dendrite development in neurons. Curr. Biol. *17*, 1752–1758.
36. Xie, Y., Vessey, J.P., Konecna, A., Dahm, R., Macchi, P., and Kiebler, M.A. (2007). The GTP-binding protein septin 7 is critical for dendrite branching and dendritic-spine morphology. Curr. Biol. *17*, 1746–1751.
37. Ewers, H., Tada, T., Petersen, J.D., Racz, B., Sheng, M., and Choquet, D. (2014). A septin-dependent diffusion barrier at dendritic spine necks. PLoS One *9*, e113916.
38. Chakravarty, A.K., Smejkal, T., Itakura, A.K., Garcia, D.M., and Jarosz, D.F. (2020). A non-amyloid prion particle that activates a heritable gene expression program. Mol. Cell *77*, 251–265, e9.
39. Jarosz, D.F., Brown, J.C.S., Walker, G.A., Datta, M.S., Ung, W.L., Lancaster, A.K., Rotem, A., Chang, A., Newby, G.A., Weitz, D.A., et al. (2014). Cross-kingdom chemical communication drives a heritable,

mutually beneficial prion-based transformation of metabolism. Cell *158*, 1083–1093.

40. Harvey, Z.H., Chakravarty, A.K., Futia, R.A., and Jarosz, D.F. (2020). A prion epigenetic switch establishes an active chromatin state. Cell *180*, 928–940, e14.
41. Itakura, A.K., Chakravarty, A.K., Jakobson, C.M., and Jarosz, D.F. (2020). Widespread prion-based control of growth and differentiation strategies in Saccharomyces cerevisiae. Mol. Cell *77*, 266–278, e6.
42. Holmes, D.L., Lancaster, A.K., Lindquist, S., and Halfmann, R. (2013). Heritable remodeling of yeast multicellularity by an environmentally responsive prion. Cell *153*, 153–165.
43. Levkovich, S.A., Rencus-Lazar, S., Gazit, E., and Laor Bar-Yosef, D. (2021). Microbial prions: dawn of a New Era. Trends Biochem. Sci. *46*, 391–405.
44. Saad, S., and Jarosz, D.F. (2021). Protein self-assembly: a new frontier in cell signaling. Curr. Opin. Cell Biol. *69*, 62–69.
45. Oamen, H.P., Lau, Y., and Caudron, F. (2020). Prion-like proteins as epigenetic devices of stress adaptation. Exp. Cell Res. *396*, 112262.
46. Cao, Q., Huang, Y.-S., Kan, M.-C., and Richter, J.D. (2005). Amyloid precursor proteins anchor CPEB to membranes and promote polyadenylation-induced translation. Mol. Cell. Biol. *25*, 10930–10939.
47. Majumdar, A., Cesario, W.C., White-Grindley, E., Jiang, H., Ren, F., Khan, M.R., Li, L., Choi, E.M.-L., Kannan, K., Guo, F., et al. (2012). Critical role of amyloid-like oligomers of Drosophila Orb2 in the persistence of memory. Cell *148*, 515–529.
48. Moore, D.L., Pilz, G.A., Araúzo-Bravo, M.J., Barral, Y., and Jessberger, S. (2015). A mechanism for the segregation of age in mammalian neural stem cells. Science *349*, 1334–1338.
49. Schindelin, J., Arganda-Carreras, I., Frise, E., Kaynig, V., Longair, M., Pietzsch, T., Preibisch, S., Rueden, C., Saalfeld, S., Schmid, B., et al. (2012). Fiji: an open-source platform for biological-image analysis. Nat. Methods *9*, 676–682.
50. Janke, C., Magiera, M.M., Rathfelder, N., Taxis, C., Reber, S., Maekawa, H., Moreno-Borchart, A., Doenges, G., Schwob, E., Schiebel, E., et al. (2004). A versatile toolbox for PCR-based tagging of yeast genes: new fluorescent proteins, more markers and promoter substitution cassettes. Yeast Chichester Engl *21*, 947–962.
51. Ferreira, P.C., Ness, F., Edwards, S.R., Cox, B.S., and Tuite, M.F. (2001). The elimination of the yeast [*PSI*$^+$] prion by guanidine hydrochloride is the result of Hsp104 inactivation. Mol. Microbiol. *40*, 1357–1369.
52. Tuite, M.F., Mundy, C.R., and Cox, B.S. (1981). Agents that cause a high frequency of genetic change from [*PSI*$^+$] to [*psi*$^-$] in Saccharomyces cerevisiae. Genetics *98*, 691–711.
53. Sharma, S.V., Agatsuma, T., and Nakano, H. (1998). Targeting of the protein chaperone, HSP90, by the transformation suppressing agent, radicicol. Oncogene *16*, 2639–2645.
54. Brown, J.C.S., and Lindquist, S. (2009). A heritable switch in carbon source utilization driven by an unusual yeast prion. Genes Dev *23*, 2320–2332.

STAR★METHODS

KEY RESOURCES TABLE

REAGENT or RESOURCE	SOURCE	IDENTIFIER
Antibodies		
Peroxidase Anti-Peroxidase Soluble Complex antibody produced in rabbit	Sigma-Aldrich	Cat# P1291, RRID: AB_1079562
Goat anti-Mouse IgG (H+L) Secondary Antibody, HRP	Life Technologies Ltd Invitrogen Division	Cat# 62-6520, RRID: AB_2533947
PGK1 Monoclonal Antibody (22C5D8)	Life Technologies Ltd Invitrogen Division	Cat# 459250, RRID: AB_2532235
DPM1 Monoclonal Antibody (5C5A7)	Life Technologies Ltd Invitrogen Division	Cat# A-6429, RRID: AB_2536204
Chemicals, peptides, and recombinant proteins		
α_1-Mating Factor acetate salt	Sigma-Aldrich	T6901
Yeast Extract	Formedium	YEA03
Peptone	Formedium	PEP03
Agar granulated	Formedium	AGR10
SC-broth 2% glucose	Formedium	CSC0201
Yeast Nitrogen Base without amino acids	Formedium	CYN0410
Complete Supplement Mixture minus uracile	Formedium	DCS0169
Complete Supplement Mixture minus histidine	Formedium	DCS0079
Complete Supplement Mixture minus adenine	Formedium	DCS0049
Complete Supplement Mixture minus tryptophane	Formedium	DCS0141
D(+) - Glucose anhydrous	Formedium	GLU03
Adenine Hemisulfate salt	Sigma-Aldrich	A3159-5G
Ammonium sulfate	Fisher scientific	A/6440/53
Casein	ACROS Organics	276071000
Deoxyribonucleic acid sodium salt from salmon testes	Sigma-Aldrich	D1626-250MG
EDTA, disodium salt	ChemCruz	sc-359904
G-418 disulphate	Formedium	G4181
Hygromycin B	Formedium	HYG5000
Nourseothricin-dihydrogen sulfate/ clonNAT powder	Werner BioAgents	5.005.000
Lithium acetate anhydrous	ACROS Organics	297110250
Guanidine Hydrochloride	Sigma-Aldrich	G40505-25
Experimental models: Organisms/strains		
S. cerevisiae: strain background S288C (BY4741). *MAT***a** *his3Δ1 leu2Δ0, ura3Δ0 met15Δ0 LYS2 ADE2 TRP1 bar1::kanMX*	This paper	yFC05
S. cerevisiae: strain background S288C (BY4741). *MAT***a** *his3Δ1 leu2Δ0, ura3Δ0 met15Δ0 bar1::kanMX, sur2::NAT*	This paper	yFC33
S. cerevisiae: strain background S288C (BY4741). *MAT***a** *his3Δ1 leu2Δ0, ura3Δ0 met15Δ0 bar1::kanMX bud6::NAT*	This paper	yFC34
S. cerevisiae: strain background S288C (BY4741). *MAT***a** *his3Δ1 leu2Δ0, ura3Δ0 met15Δ0 bar1::kanMX bud1::NAT*	This paper	yFC35

(*Continued on next page*)

Continued

REAGENT or RESOURCE	SOURCE	IDENTIFIER
S. cerevisiae: strain background S288C (BY4741). *MAT***a** *ura3 his3 leu2 met15 WHI3-3GFP:kanMX bar1::HIS3*	This paper	yFC13
S. cerevisiae: strain background S288C (BY4741). *MAT***a** *bud1::NatMX bar1:kanMX Whi3-3GFP:kanMX*	This paper	yFC20
S. cerevisiae: strain background S288C (BY4741). *MAT***a** *bud6::NatMX bar1:kanMX Whi3-3GFP:kanMX*	This paper	yFC21
S. cerevisiae: strain background S288C (BY4741). *MAT***a** *sur2::NatMX bar1:kanMX Whi3-3GFP:kanMX*	This paper	yFC22
S. cerevisiae: strain background S288C (BY4741). *MAT***a** *his3Δ1 ura3Δ0 leu2Δ0 met15Δ0 Sec61-mCherry:kanMX WHI3:m-neongreen:NatMX bar1:kanMX*	This paper	yFC203
S. cerevisiae: strain background W303. *MATα leu2-3,-112 his3-11,-15 trp1-1 ura3-1 ade1-14 can1-100 [RNQ$^+$] [PSI$^+$]*	Jonathan Weissman	N/A
S. cerevisiae: strain background W303. *MATα leu2-3,-112 his3-11,-15 trp1-1 ura3-1 ade1-14 can1-100 sur2::HIS3 [RNQ$^+$] [PSI$^+$]*	This paper	yYB8435
S. cerevisiae: strain background S288C (BY4741). *MAT***a** *his3Δ1 leu2Δ0 met15Δ0 ura3Δ0 bar1::kanMX sur2::NatMX Whi3-GFP:HIS3MX6*	This paper	yFC38
S. cerevisiae: strain background W303 *MAT***a/alpha** *SUP35/SUP35-GFP:HIS3 leu2-3,-112/leu2Δ0 his3-11,-15/his3Δ1 trp1-1/TRP1 ura3-1/ura3Δ0 ade1-4/ADE1 can1-100/CAN1 MET15/met15Δ0 SEC61/Sec61:mCherry:URA3 [RNQ$^+$] [PSI$^+$]*	This paper	yFC202
S. cerevisiae: strain background W303 *MAT***alpha** *leu2-3-112 his3-11,-15 trp1-1 ura3-1 ade1-4 can1-100 pRS304 pGPD GST-UGA-GFP-pest:URA3 [RNQ$^+$] [PSI$^+$]*	This paper	JS407
S. cerevisiae: strain background W303 *MAT***alpha** *leu2-3-112 his3-11,-15 trp1-1 ura3-1 ade1-4 can1-100 sur2::KanMX pRS304 pGPD GST-UGA-GFP-pest:URA3 [RNQ$^+$] [PSI$^+$]*	This paper	JS681
Recombinant DNA		
LEU2 pCUP1::SPC42-GBP-RFP CEN6 ARS209	Thorpe group[25]	PHT11
Software and algorithms		
FIJI	[49]	https://imagej.net/software/fiji/
Graphpad Prism 9.3.0	GraphPad Software Inc.	https://www.graphpad.com/scientific-software/prism/

RESOURCE AVAILABILITY

Lead contact

Further information and requests for reagents and resources should be directed to and will be fulfilled by the lead contact, Fabrice Caudron (fabrice.caudron@igmm.cnrs.fr).

Materials availability

Yeast strains generated in this study are available through the lead contact, Fabrice Caudron.

Data and code availability

All data reported in this paper will be shared by the lead contact, Fabrice Caudron upon request.

This paper does not report original code.

Any additional information required to reanalyze the data reported in this paper is available from the lead contact upon request.

EXPERIMENTAL MODEL AND SUBJECT DETAILS

Yeast strains and growth

Strains used for escape from pheromone arrest were derivatives of the s288c BY4743 wild type with deletions obtained according to Janke et al.[50] W303 strains used to test for [*PSI*$^{+}$] induction and curing were obtained from Jonathan Weissman. Localisation of Whi3 in *CE*$^{sur2\Delta}$ was analysed in strain yFC38. To analyse co-localisation of Sup35-GFP and Sec61-mCherry we used strain yFC202. For stop codon readthrough, we used wild type or *sur2Δ* strains with integrated *pGPD GST-UGA-GFP-pest:URA3.* The plasmid to express *SPC42-GBP* was obtained from the Thorpe group and is PHT11 from Ólafsson and Thorpe.[25]

Cells were grown on rich medium (Yeast Extract, Peptone, 2% Dextrose, Formedium) at 30°C in a shaking incubator (200 rpm). To obtain cells in exponential phase of growth, an overnight preculture was diluted to OD_{600nm} 0.2 and grown for 4 hours before the experiment. For live cell fluorescence microscopy, cells were grown on SC -TRP (Formedium).

METHOD DETAILS

Yeast strains constructions

Generally, gene deletions were obtained through homologous recombination with cassettes amplified from plasmids from Janke et al.[50] We used standard lithium acetate transformation and growth on selective media. Single colonies were streaked out on selective media and the genotype was confirmed by diagnostic PCR (integration of the cassette and loss of the endogenous locus).

Strains used for Whi3 localization were derivatives of the wild type backcrossed in mutant strains. Strains for the co-localization of Whi3-3GFP and Sec61-mCherry were obtained by PCR tagging of *SEC61.*

Microscopy

All images were acquired either on a Personal Deltavision (Applied Precision) equipped with a CCD HQ2 camera (Roper) and 250W Xenon lamps controlled by Softworx or a Deltavision Elite (GE Healthcare) equipped with a sCMOS camera and solid-state light-emitting diodes controlled by Softworx. Fluorescein isothiocyanate and tetramethylrhodamine isothiocyanate filters were used for imaging GFP and mCherry fluorescence. Deconvolution was performed using Softworx.

Microfluidics

Experiments were carried out with the ONIX microfluidic perfusion platform with Y04C microfluidic plates (CellAsic). Medium was yeast extract peptone dextrose (YPD) supplemented with 20 μg/ml casein and containing 7 nM α-factor. α-factor was aliquoted in 10μl samples at 1mg/ml with 20 μg/ml casein and aliquots were used only once.

General information for peptide synthesis

HMPB-ChemMatrix was purchased from Biotage (Uppsala, Sweden). All classical side chain protected amino acids were purchased from Bachem. They are listed in Table S2. HATU was purchased from Aapptec (Louisville, USA) and all other chemicals were purchased from Sigma Aldrich (Merck KGaA, Darmstadt, Germany). All reagents were used as received; solvents were technical grade.

Peptide couplings were carried out in ISOLUTE double fritted filtration columns, 15 or 25 mL (*reaction vessel*, Biotage) with orbital shaking at 600-700 rpm at RT. The building blocks for peptide synthesis were activated in 20 mL brown glass storage vials (27x57 mm, *activation vessel*, Infochroma ag) closed with Teflon lined at RT.

MALDI-TOF mass spectra (MALDI-TOF MS) were recorded on a Brucker microflex benchtop MALDI-TOF system. High-resolution mass spectrometry (HRMS) was performed on a Bruker maXis UHR-TOF by electrospray ionization (ESI) by the Molecular and Biomolecular Analysis Service (MoBiAS) of the LOC at ETH Zurich.

Analytical HPLC conditions for peptide analysis

All analytical HPLC runs were performed with a Dionex Ultimate 3000 system equipped with a 3000 pump-module, a 3000 Autosampler, a 3000 RS Variable Wavelength Detector, and a Xbridge C18 3.5 μm 150x4.6 mm column (Waters) The eluent system was a mixture of H_2O and ACN containing 0.1% TFA. The condition used is summarized in Table S3.

Semi-preparative HPLC conditions for peptide purification

All semi-preparative HPLC runs were performed with a Waters preparative 150 LC system equipped with a 2545 quaternary gradient module, a 2489 UV/visible detector, a Fraction Colector III and a Reprosil Gold 120 C18 5 μm 250x20 mm column (Morvay Analytik). The eluent system was H_2O and ACN both supplemented with 0.1% TFA.

Lyophilized peptidic samples were always dissolved in a solvent mixture identical to that at the beginning of the purification gradient. In some cases, drops of MeOH or DMF were added to help solubilization. Every sample was filtered through a 0.22 μm filter before injection on the semi-preparative column. For the exact separation conditions refer to the detailed synthesis protocol of the individual peptides.

Different gradients were used with a flow rate of 15 mL/min. A list of the different gradient used can be found in Table S4.

General protocol (GP1) for coupling the first amino acid to free acid linker (0.1 mmol scale)

In a 25 mL *reaction vessel* equipped with a valve and attached to a suction system, a resin with free acidic linker (0.1 mmol) was shaken in DMF for 30 min. The resin was then treated with 20% (vol/vol) piperidine-DMF (5 mL) for 5 min and washed with DMF (5x 1 min, 5 mL each). In a 10 mL *activation vessel*, the Fmoc-protected amino acid of choice (0.6 mmol, 6 eq.) was dissolved in 0.4 M HATU in DMF (1360 μL, 0.54 mmol, 5.4 eq.) and DIPEA (187 μL, 10.8 mmol, 10.8 eq.) and activated for 2 min at RT. Afterwards, the solution was transferred to the *reaction vessel* and 1 mL of 10 mg/mL DMAP in DMF was added. The reaction was shaken overnight at RT. Finally, the resin was washed with DMF (5x 1 min, 5 mL each), treated for 5 min with DMF-Ac_2O-DIPEA (10 mL, 8:1:1) and washed again with DMF (5x 1 min, 5 mL each). The resin was then stored at 4 °C until further use (usually within 2 weeks).

GENERAL PROTOCOL (GP2) FOR MANUAL FMOC SPPS WITH 6 EQ. AMINO ACID (0.1 MMOL SCALE)

In a 25 mL *reaction vessel* equipped with a valve and attached to a suction system, the resin loaded with the first Fmoc-protected C-terminal amino acid (0.1 mmol) was shaken in DMF for 30 min. The resin was then treated with 20% (vol/vol) piperidine-DMF (5 mL) for 5 min and washed with DMF (5x 1 min, 5 mL each). Peptide chain assembly was performed as described in Table 5. The only exception was for the coupling of the first amino acid, which was carried out for 2h. Finally, theresin was treated with CH_2Cl_2(5x 1 min washes, 5 mL each),dried undersuction for 25 min and transferred to a flask suitable for resin cleavage. The dried resin was either cleaved directly or stored at -20 °C.

General cleavage protocol (GP3)

In a round-bottom flask, the dried resin was swollen in TFA-ddH_2O-TIS (95:2.5:2.5; 20 mL/mg dry resin). The mixture was stirred at RT for at least 2h. Afterwards, the resin was filtered using a fritted glass filter and washed with 2-3 mL neat TFA. The TFA was evaporated with N_2 flow until some material started to precipitate. Then, 4 °C Et_2O was added and the resulting suspension was filtered on celite and rinsed with 4 °C Et_2O to remove cleaved protecting groups. To solubilize the peptidic material, the celite was resuspended in H_2O-ACN + 0.1% TFA (3x, 40 mL each, 1:1) and filtered. The filtrate was frozen, lyophilized and stored at 4 °C before purification via semi-preparative HPLC.

Whi3^{polyQ} (H-SQQQSQQQQQQPQQPQQHSTQKHSPQQCNQQQVNSSIPLSSQGQ-OH)

Whi3^{polyQ} was synthesized on a 0.1 mmol scale on HMPB-ChemMatrix (225 mg, 0.44 mmol/g). The first amino acid was coupled according to **GP1** and the rest of the synthesis followed **GP2**. The cleavage was carried out as described in **GP3**. The crude product was purified via semi-preparative HPLC with gradient 1. Fractions were analyzed with MALDI-TOF MS and analytical HPLC, combined according to purity and lyophilized. Pure Whi3^{polyQ} was obtained as a white powder. The corresponding analytical chromatogram is shown in Figure S6. HRMS analysis of the produced peptide delivered the expected mass.

HRMS (ESI): deconvoluted calculated at 5010.3268, found 5010.3165.

B2M^{K3} (H-SNFNLCYVSGFHPSDIEVDLLK-OH)

B2M^{K3} peptide was synthesized on a 0.1 mmol scale on HMPB-ChemMatrix (225 mg, 0.44 mmol/g). The first amino acid was coupled according to **GP1** and the rest of the synthesis followed **GP2**. The cleavage was carried out as described in **GP3**. The crude product was dissolved in 7 M GuHCl + 0.1% TFA and purified via semi-preparative HPLC with gradient 2. All interesting fractions were analyzed with MALDI-TOF MS and analytical HPLC, combined according to purity and lyophilized. Pure B2M^{K3} was obtained as a white powder. The corresponding analytical chromatogram is shown in Figure S6. HRMS analysis of the produced peptide delivered the expected mass.

HRMS (ESI): deconvoluted calculated at 2497.2024, found at 2497.1788.

Fiber growth

In order to grow fibers, pure lyophilized peptide samples (for Whi3^{polyQ}) or DMSO stock (10 mM/mL for B2M^{K3}) were diluted to the desired concentration with growth buffer (25 mM NaH_2PO_4. 150 mM NaCl, pH 7.4 + 0.05% (w/w) NaN_3) in 1.5 mL Eppendorf tubes. The tubes were then sonicated for 10 min in a sonication bath (Telesonic Ultrasonics TPC-40). Afterwards, they were incubated at 30 °C and 470 rpm on an incubating microplate shaker (VWR) equipped with a rack for Eppendorf tubes.

Seed production and seeding

To produce seeds, preformed fibers were sonicated for 1 to 5 min in a sonication bath (Telesonic Ultrasonics TPC-40). In the case of diluted seed solution, the sonication step was carried out with samples at their original concentration and diluted afterwards. To start a seeding experiment, the original seed solution was diluted 10x in fiber growth buffer containing unaggregated peptide.

Fluorescence spectroscopy

Fluorescence spectra were recorded on a PTI QM-7SE spectrofluorometer using a 1.0 cm × 0.2 cm cuvette (Hellma® fluorescence cuvettes, Micro (Suprasil® quartz)). The samples for measurements were prepared by adding 10 μL aliquot of the amyloid solution to 490 μL of 20 μM dye in growth buffer (25 mM NaH_2PO_4. 150 mM NaCl, pH 7.4 + 0.05% (w/w) NaN_3). The excitation wavelength used for every dye as well as the spectral range recorded are summarized in Table S6. Emission spectra were recorded at 25 °C in 2 nm steps with 1 s integration and averaged 3 times.

Amyloid fiber growth monitoring

The growth of amyloid fibers was monitored by measuring the difference in bisANS fluorescence at 494 nm between a sample containing peptides (prepared as described in the fluorescence spectroscopy protocol above) and a blank. The value obtained were then normalized and plotted.

Electron microscopy

Formvar/carbon 400 mesh copper EM grids (Ted Pella Type B 01814-F) where treated with negative N_2 plasma for 60 s at 25 mA. Afterwards, one sample drop (4 μL) was placed on the grid and incubated for 1 min. The grid was then dried with blotting paper, washed twice with deionized H_2O, with successive drying between each step. Finally, the sample was washed briefly with 2% (w/v) uranyl acetate, dried by blotting, and subsequently stained for 20 s with a second droplet of the same solution. The grid was then blotted and air dried before analysis (sometimes many days/weeks after grid preparation). All electron micrographs were collected using a JEM-1400 Plus (JEOL) with an accelerating voltage of 120 keV. Width of fibers were measured from EM micrographs with a magnification of 100 kX and analyzed with Photoshop (Adobe, version CS6 and CS10).

Inheritance on the CE phenotype during meiosis

Consistent with their extensive resistance to pheromone treatment, crossing CE to wild type cells was inefficient. However, we could backcross some of them. Meiosis gives rise to 4 spores, 2 of which are *MAT*α and 2 *MAT***a**. Therefore, we expected that out of 4 spores, 2 would always grow on alpha-factor because they are *MAT*α. In wild type cells, the 2 other spores do not grow on alpha-factor (0.6μM, Figure S2). If in the CE more than 2 spores were growing, it would mean that they had inherited the CE phenotype. If the CE is due a mutation that is unlinked to the *MAT* locus, 4/6 of the tetrads should have 3 spores growing on alpha-factor containing medium, 1/6 should contain 4 such spores and the last 1/6 of the tetrads should contain only 2 of them (pattern #1). If it is due to a mutation linked to the *MAT* locus, the fraction of tetrads with 3 and 4 spores growing on alpha-factor containing medium should be increased (pattern #2). In case of a non-mendelian factor propagating through meiosis, all tetrads should contain 4 spores growing on alpha-factor containing medium (pattern #3). Finally, a non-mendelian factor that does not pass meiosis should produce tetrads with always only 2 spores growing on alpha-factor containing medium (pattern #4). We backcrossed 13 independent CE strains and tested the growth of each spore on alpha-factor (0.6μM). For 4 backcrosses, we observed tetrads in which 2, 3 or 4 spores out of 4 were growing on α-factor (Figure S2). These backcrosses fall in the pattern #1, suggesting the presence of a single 'sterile' mutation segregating independently from the mating type locus. In 4 other backcrosses, the majority of the tetrads contained 2 spores and few 3 spores growing on alpha-factor containing medium, most compatible with the pattern #4. Furthermore, 5 backcrosses followed strictly pattern #4 (Figure S2). Thus, the last 9 backcrosses, which are not compatible with a single mutation, suggests that the CE phenotype is due to non-mendelian factor that is lost during meiosis.

Curing of the CE phenotype

We isolated 31 $CE^{sur2\Delta}$ and passaged them three times on YPD, YPD supplemented with guanidine hydrochloride (3 mM) to inhibit Hsp104[51,52] or YPD supplemented with radicicol (10μM) to inhibit Hsp90.[53] In addition, we transformed all 31 $CE^{sur2\Delta}$ and the parental *sur2Δ* strain with a dominant negative allele of *SSA1* ($SSA1^{DN}$, [39,54]). In all cases, after 3 passages the 31 $CE^{sur2\Delta}$ were still able to grow on YPD containing pheromone (0.6μM), while the parental *sur2Δ* strain was not (Figure S2). However, upon microscopic observation of $CE1^{sur2\Delta}$, we found that many cells were shmooing and other dividing. This was not the case for other $CE^{sur2\Delta}$, and it was also not the case for $CE1^{sur2\Delta}$ passaged on YPD without drugs or with GuHCl or radicicol (Figure S2). Therefore, the CE phenotype is not cured by either GuHCl, radicicol or passages for many generations on YPD, but one variant was partially cured upon inhibition of the Hsp70 chaperone Ssa1.

Microsome fractionation

Cell cultures in YPD ±pheromone were spun down at 600g for 2 minutes. Cell pellets were resuspended in 400μl of ice-cold lysis buffer (50 mM Tris, pH 7.5, 100 mM NaCl, 2.5mM EDTA, 1% (v/v) Triton X-100, 2mM PMSF, 20mM NEM and 1 tablet of protease inhibitor cocktail per 10ml of buffer) in screw cap tubes. Acid washed glass beads (filling a 200μl pcr tube) were added to each tube abd cells were lysed using a FastPrep tissue homogenizer (MP Biomedicals) for 30s followed by 1 min on ice. Homogenization

was repeated 5 times in total. Tubes were kept on ice for 20min and centrifuged at 300g for 2min at 4°C. Supernatants were transferred into fresh tubes (±400µl) and spun at 25,000 rpm for 30min at 4°C (Beckman Optima L-80XP). The supernatant was collected and the pellet was resuspended in 200µl of lysis buffer. Laemli buffer was added to the samples which were heated at 95°C for 5min.

QUANTIFICATION AND STATISTICAL ANALYSIS

All statistical analyses were obtained using Graphpad Prism 9.3.0, except for the refined analysis of CE frequencies (see below). Sample numbers of cells n for all experiments are included within their respective figure legends and methods and were collected over a minimum of three biological replicates.

QUANTIFICATION OF SHMOOING

Shmooing or budding states were inspected visually. During microfluidic experiments, images were taken every 15 min. Unbudded cells that showed a polarized growth were counted as shmooing. Unbudded cells undergoing isotropic growth were counted as G1 cells. Usually, these cells soon started forming a bud. Samples consisted of three independent clones.

QUANTIFICATION OF WHI3-3GFP SUPER-ASSEMBLIES

Cells were grown in YPD supplemented with 20 mg/ml casein and containing 7 nM α-factor and were briefly centrifuged at 600 g, resuspended in SD-TRP medium, placed between slide and coverslip, and imaged immediately. Images were analyzed after deconvolution with Softworx software as before.[27] A super-assembly is counted when a brighter region of fluorescence is detectable on more than 2 focal planes (spaced by 300nm). Three clones with total n > 122 cells were observed for each strain.

Quantification of [*PSI+*] *de novo* appearance

[*PSI*$^+$] wild type and *sur2Δ* cells were first cured with 3 passages on YPD agar medium containing 3 mM GuHCl. Red single colonies [*psi*$^-$] were assessed for their ability to become white again. Cells were plated on SC-Ade and YPD and the frequencies of appearance of white colonies were measured. White colonies were tested for their ability to become red again after passages on YPD containing 3 mM GuHCl. In all tested cases, colonies became red again, demonstrating that white colonies were indeed [*PSI*$^+$].

Quantification of [PSI+] curing during treatment with GuHCl

Cells were grown overnight in liquid YPD and diluted in the morning to OD_{600nm} = 0.2 in YPD with 3 mM GuHCl. Samples were taken every 30 minutes and plated on synthetic medium with low adenine concentration. Liquid cultures were kept in exponential phase during the experiment. Colonies were allowed to grow at 30°C for several days and the proportion of white and red colonies was assessed after 2 days of incubation at 4°C to allow for the red colour to develop well. We initially determined that curing started to happen after 12 hours of GuHCl treatment for both wild type and *sur2Δ* strains.

Quantification of Stop-codon read-through by flow cytometry

For the stop codon read through experiments, wild-type [*PSI*$^+$] and *sur2Δ* [*PSI*$^+$] cells expressing chromosomally integrated pGPD GST-UGA-GFP-pest were grown for 5 hours without GuHCl or with 0.1mM or 1mM GuHCl. The GFP fluorescence intensity was measured with a BD Accuri C6 Flow Cytometer using 488 nm laser and 533/30 BD filter for 100 000 cells/ clone (3 clones each). The data was analyzed using FlowJo software (FlowJo LLC).

Cell sizes measurements

Cell sizes were determined using a CASY cell counter model TTC (Schärfe system). Strains were grown to early log phase, diluted in CASYton (Electrolyte buffer from Schärfe system) and processed according to the manufacturer instructions. For the *WHI3* reintroductions experiments (Figure S3E), cell length was measured using FIJI[49] tracing a line in the mother cell longest axis.

Quantification of Sup35 foci and Whi3 super-assemblies/foci/granules co-localisation with ER membranes

For Whi3-3GFP localisation, cells were grown in YPD supplemented with 20 mg/ml casein and containing 7nM α-factor and were briefly centrifuged at 600 g, resuspended in SC-TRP medium, placed on a SC-TRP agar pad covered by a coverslip, and imaged immediately. Images were analysed after deconvolution with Softworx software. Three clones with total n = 194 cells, 250 cells, 170 cells and 153 cells for 3 hours, 4 hours, 6 hours and 10.5 hours condition were observed for each strain. A total of 333, 402, 393 and 317 super-assemblies were analysed at 3 hours, 4 hours, 6 hours and 10.5 hours' time points. Note that we only analysed super-assemblies that were in the 5 best focal planes as co-localisation was difficult to assess on the top and bottom focal planes and we only counted Sup35-GFP foci and Whi3-3GFP super-assemblies in the mother cells. We considered that Whi3 assemblies co-localised with the Sec61-GFP signal if overlapping or immediately adjacent pixels were observed.

Quantification and analysis of CE frequencies

Diploid strains heterozygous for the different mutations were sporulated (for example *SUR2*/*sur2Δ* or *WHI3*/*whi3Δ*). *MAT***a** spores were selected and their genotypes determined by growth on selection media. At least 44 independent spores carrying each individual mutation were tested. Strains were grown in YPD until mid-log phase and spotted on solid YPD and solid YPD containing 0.6µM α-factor. Colonies were counted after 2-3 days of growth at 30°C.

The analysis was conducted on the estimates of the of relative yeast density obtained from the colony count (C) at an appropriate dilution (D). The relative density for each clone was obtained in the presence of the pheromone (p) and the corresponding control (c), so the relative performance is given by the ratio:

$$R = CpDp/CcDc$$

The ratio was logit transformed in an attempt to standardize the variance. Having fitted the average for each yeast strain, the residuals were clearly strongly asymmetrical (Figure S7 shows the deviation from a cumulative normal distribution). This pattern might be expected if in a subset of cases the constitutive escaper phenotype occurred early in the culture. The departure from a cumulative normal distribution of residuals is abrupt for standardized residuals greater than one (shown by the vertical line). Since the incidence of these outcomes did not differ between strains ($\chi^2 = 3.02$, P = 0.88) they were excluded from subsequent analysis of the ratios.

Figure 5C shows the distribution of the logit transformed ratios (R) for each genotype. A linear model describing the means of each strain, showed a highly significant difference between the three strains for which there were a priori expectations of a stronger effect of the pheromone (*WHI3-ΔpQ*, *bud1Δ WHI3-ΔpQ* and the wildtype) and the remainder (ANOVA P < 2e-16). The fitted values for these two categories is shown by the red line. There were no significant differences between the means for this remaining group (P = 0.41) whereas there were significant differences among the three (P < 0.0007) - in particular *WHI3-ΔpQ* was markedly lower than the wild type (P<0.0008). The R package for this analysis is available in Methods S1.